The author is very grateful to Professor N. Kato of Nagoya University for continuously guiding him and discussing the subject of the present paper and related problems.

References

BECKER, P. J. & COPPENS, P. (1973). First Eur. Crystallogr. Meet., Bordeaux, France.
BECKER, P. J. & COPPENS, P. (1974*a*). *Acta Cryst.* A**30**, 129-147.
BECKER, P. J. & COPPENS, P. (1974*b*). *Acta Cryst.* A**30**, 148-153.
BECKER, P. J. & COPPENS, P. (1975). *Acta Cryst.* A**31**, 417-425.
COPPENS, P. & HAMILTON, W. C. (1970). *Acta Cryst.* A**26**, 71-83.
KATO, N. (1976*a*). *Acta Cryst.* A**32**, 453-457.
KATO, N. (1976*b*). *Acta Cryst.* A**32**, 458-466.
KATO, N. (1980*a*). *Acta Cryst.* A**36**, 763-769.
KATO, N. (1980*b*). *Acta Cryst.* A**36**, 770-778.
KATO, N. (1982). *Z. Naturforsch. Teil A*, **37**, 485-489.
TAKAGI, S. (1962). *Acta Cryst.* **15**, 1311-1312.
TAKAGI, S. (1969). *J. Phys. Soc. Jpn*, **26**, 1239-1253.
THORNLEY, F. R. & NELMES, R. J. (1974). *Acta Cryst.* A**30**, 748-757.
ZACHARIASEN, W. H. (1967). *Acta Cryst.* **23**, 558-564.

Acta Cryst. (1986). A**42**, 469-478

Accurate Measurement of the Si Structure Factor by the *Pendellösung* Method

BY T. SAKA* AND N. KATO†

The Department of Crystalline Materials Science, Faculty of Engineering, Nagoya University, Chikusa-ku, Nagoya, Japan

(*Received* 18 *February* 1986; *accepted* 16 *April* 1986)

Abstract

The X-ray structure factor of Si was measured for 30 net planes from the thickness dependence of the integrated intensity on the λ scale. In ten low-order planes, the accuracy level was estimated to be 0·05% in the probable error. Therefore, the deviation from the standard model of Hartree-Fock isolated atoms under harmonic oscillation could be determined with high precision. In the remaining net planes, the accuracy level was 0·1%. Dawson's rule (that even and higher-order reflections should be normal) was well satisfied for eight net planes higher than 660. Against this background, some F_g values of odd and middle-order planes deviate from the standard model. In the difference Fourier map, not only the bonding charge and the charge deficit in the anti-bonding region but also a slight excess near the atomic position were recognized.

1. Introduction

The accurate structure factor (F_g) in X-ray diffraction gives valuable information on electron distribution in crystals. At present, the highest accuracy on the absolute scale is obtained in Si by the *Pendellösung* method, using the fact that the X-ray intensity field oscillates with either a spatial or an angular period which is proportional to $|F_g|^{-1}$.

Since the first experiment (Hattori, Kuriyama, Katagawa & Kato, 1965), several groups have attempted a more accurate measurement and explored the methodology as well as the underlying theory. The earlier work was reviewed by Kato (1969); at that stage, the accuracy level was about 0·5% in the probable error. Tanemura & Kato (1972) and the extensive work of Aldred & Hart (1973*a*, *b*) advanced the accuracy level to approximately 0·1%. 15 net planes were measured in the latter work. In these experiments, essentially *Pendellösung* fringes in the section topograph were used. Although the experimental set-up was extremely simple, its disadvantage lies in the need for a large well defined wedge of perfect crystal.

Several modifications were proposed to overcome this disadvantage. Takama, Iwasaki & Sato (1980) used the λ dependence of the integrated intensity on the λ scale, and Utemisov, Somenkova, Somenkov & Shil'shtein (1980) and Utemisov, Shil'shtein & Somenkov (1981) used the t dependence of the integrated intensity on the θ scale, where t is the effective thickness and can be continuously changed by rotating the azimuthal angle φ with the Bragg condition fixed. More recently, Teworte & Bonse (1984) used the intensity oscillation in the high-

* Present address: Central Research Laboratory, Daido Steel Co., Ltd, 2-30 Daido-cho, Minami-ku, Nagoya, Japan.
† Present address: Department of Physics, Meijo University, Shiogmaguchi, Tempaku-ku, Nagoya, Japan.

0108-7673/86/060469-10$01.50

precision rocking curve and presented an accurate data set of $|F_g|$ to the same level of accuracy as that of Aldred & Hart (1973*a*, *b*).

In the present work, 30 net planes were measured. The principle is similar to that of Utemisov *et al.* (1980), except that continuous X-rays were used instead of the characteristic rays. In other words, the t dependence of the integrated intensity on the λ scale was used. Also, we used X-rays of short wavelength (~0·4 Å). Thus, besides the feasibility of determining accurately the oscillation period, many net planes could be measured. Moreover, the amount of correction for anomalous dispersion could be reduced. Thus, the $|F_g|$ values after correction were estimated to be accurate at the 0·05% level of error in the ten lower-order reflections and at the 0·1% level in 20 other reflections.

This paper concerns the methodological aspects rather than the physical implications of our results. Nevertheless, the data set was examined based on Dawson's (1967*a*) formalism of the general structure factor. Also, the difference Fourier synthesis was applied to the original data set and a reasonable electron density could be obtained.

2. The theoretical background

The present method is based on the thickness (t) dependence of the integrated intensity on the λ scale, which is proportional to the ordinary integrated intensity on the angular scale in the rocking curve or that on the spatial scale in the transverse topograph. For the σ mode of X-ray polarization and the symmetrical Laue case, the expression apart from an irrelevant proportional constant has the form (Kato, 1968)

$$R_\sigma(t) = |F_g|[W(\xi) + I_0(\eta) - 1]A(t) \qquad (2.1)$$

where W is defined by the Bessel function J_0 as

$$W(\xi) = \int_0^\xi J_0(\rho)\, d\rho, \qquad (2.2)$$

I_0 is the modified Bessel function and $A(t)$ is the normal attenuation factor having the form

$$A(t) = \exp(-\mu_0 t/\cos\theta_B). \qquad (2.3)$$

Here, μ_0 and θ_B are the linear absorption coefficient and the Bragg angle, respectively. ξ and η in (2.1) are defined by

$$(\xi + i\eta) = 2(r_c\lambda/v)(F_g F_{-g})^{1/2}(t/\cos\theta_B) \qquad (2.4)$$

where r_c is the classical radius of the electron, λ is the wavelength, v is the unit-cell volume, and F_g is the structure factor including the temperature effect.

The complex nature of $\xi + i\eta$ arises from $(F_g F_{-g})^{1/2}$. If one neglects the minute effect of the imaginary part of F_g in the case of centrosymmetric crystals like Si, the real part of $(F_g F_{-g})^{1/2}$ and $|F_g|$ need not be distinguished (*e.g.* Azaroff, 1974). Then ξ is given by the same equation as (2.4) with $|F_g|$ instead of $(F_g F_{-g})^{1/2}$.

Under the approximation of the standard spherical model (SSM) of the charge distribution and the harmonic thermal vibration,

$$F_g = Q(f_0 + f' + if'')\exp(-M), \qquad (2.5)$$

where $Q = 8$ (even reflections) and $4(2)^{1/2}$ (odd reflections) with an appropriate sign for the diamond structure, and $\exp(-M)$ is the Debye–Waller factor. More details will be given in § 6.1.

For the π polarization mode, the integrated intensity R_π is given simply by substituting $F_g \cos 2\theta_B$ instead of F_g in (2.1) and (2.4).

For the accurate determination of $|F_g|$ one needs accurate values of the physical and material constants. In the present work the following values were employed.

$$r_c = 2{\cdot}8178 \times 10^{-13}\ \text{cm} \qquad (2.6a)$$

$$a = 5{\cdot}4310 \times 10^{-8}\ \text{cm} \qquad (2.6b)^*$$

$$\mu_0 = 2{\cdot}84\ \text{cm}^{-1} \quad (\text{for } \lambda = 0{\cdot}4\ \text{Å}) \qquad (2.6c)$$

$$M = 3{\cdot}90 \times 10^{-3}(h^2 + k^2 + l^2). \qquad (2.6d)^\dagger$$

For later purposes (§§ 4.3 and 5.2) one technical matter is mentioned here. R_σ and R_π are functions of t. The behaviour of the *Pendellösung* oscillation, however, is essentially determined by $W(\xi)$ in (2.1). If one writes

$$\xi = 2\pi(t/\Lambda), \qquad (2.7)$$

Λ is the spatial period of the oscillation. Then one can write

$$\eta = [f''/(f_0 + f')]\xi, \qquad t = [\Lambda/2\pi]\xi. \qquad (2.8a,b)$$

Since $I_0(\eta)$ and $A(t)$ are slowly varying functions, in these expressions, one can use the approximate but fixed values f_0, f' and f'' and Λ based on (2.5). In this way, $R_{\sigma,\pi}(t)$ can be regarded as functions of ξ.

Finally, the theoretical curve which meets the observation is assumed to be

$$R(\xi) = \tfrac{1}{2}(1 - D)R_\sigma(\xi) + \tfrac{1}{2}(1 + D)R_\pi(\xi) \qquad (2.9)$$

where ξ is given by (2.7), and D is the degree of polarization of the incident beam. We shall have more to say in § 5.2 about the X-ray polarization.

3. Experimental

3.1. *Specimens*

Five specimens were prepared from FZ silicon wafers supplied by a semiconductor company. Table 1 shows the growth direction and the surface index.

* Hart (1981).

† We shall use a more accurate value later, when it is necessary.

Table 1. *The specification of specimens*

Specimen No.	Growth direction	Surface	Thickness (μm)
I	[001]	(112)	700·2
II	[001]	(112)	700·2
III	[001]	(001)	697·4
IV	[011]	(011)	1201·5
V	[011]	(011)	702·6

The surface was finished by mechanochemical polishing. The wafer was scratched by a glass cutter and cleaved along {111} planes into pieces of about 15 mm square. The strain induced during these processes was removed by chemically etching the cleaved surfaces for about 5 min. The etchant was a solution of HF and HNO_3 (1:9 in volume ratio). The flatness of the specimen surface was checked by optical interferometry.

The thickness T of the specimen was measured by a contact method (Digitaler Messtaster MT30) after the X-ray experiment with an accuracy of 0·2 μm, which amounts to a relative error of 0·03%. Table 1 also includes the thickness of each specimen.

3.2. *X-ray apparatus*

Fig. 1 shows schematically the experimental arrangement. Continuous X-rays from a high-intensity generator (RU-1500) were used as the incident beam. The accelerating voltage and beam current were 50 kV and 1200 mA, respectively, in the standard experiment. Both Ag and Cu targets were used. The beam size was 1·2 mm in diameter and about 10′ in angular divergence. Specimens were mounted on an automatic four-circle goniometer. The minimum stepping angle of the φ axis was 0·00125°.

The energy spectrum of the Bragg-reflected beam was measured by a solid-state detector (SSD) of pure Ge, the energy resolution being 199 and 487 eV at 5·9 and 122 keV, respectively. A receiving aperture of 3 mm diameter was put in front of the detector and air scattering was carefully eliminated. The data were recorded first in a 1024 multi-channel analyser (MCA) and transferred to floppy disks. The goniometer, MCA and floppy disk were operated by a microcomputer.

3.3. *The integrated intensity*

The specimen was set vertically under the symmetrical Laue condition, the scattering vector being parallel to the φ axis, which was set horizontally. The effective thickness t was changed by φ scanning over ±60° through the vertical position ($\varphi = 0^0$). The minimum stepping angle is equivalent to a thickness change of 0·08 μm for a 1 mm specimen at 60°.

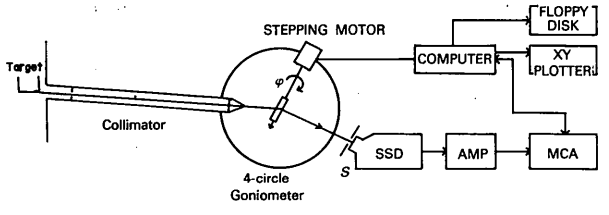

Fig. 1. The experimental set-up.

In each specimen, the measurement was carried out for as many available net planes as possible. It is worth mentioning that a set of measurements was performed without detaching the specimen from the goniometer head so that nearly the same part of the specimen could be used. The integrated intensity (R) of each reflection was obtained by summing the numbers of photons symmetrically over ±30–50 channels on both sides of the peak channel of the MCA.

The wavelength was fixed at 0·4 Å in the standard case.* The other spectral lines were used only for a study of the λ dependence of the structure factor (anomalous dispersion) and the calibration of the MCA (see § 4.2).

Typical curves of R *versus* $(\cos\varphi)^{-1}$ are shown in Fig. 2 for lower- (a), medium- (b) and higher-order reflections (c). The *Pendellösung* oscillation is clearly observed. Whereas the behaviour of the integrated intensity could be well described by the dynamical formula for R (2.9) in the case (a), the curve averaged over oscillations is nearly constant in (b) and increases with increasing $(\cos\varphi)^{-1}$ in (c).

* In the case of 555, 0·415 Å was used.

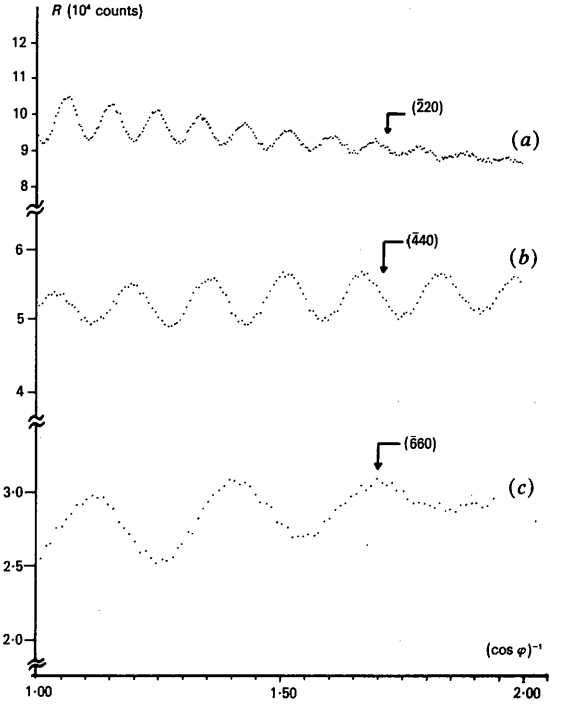

Fig. 2. Typical examples of $R(\varphi)$ for lower- (a), middle- (b) and higher-order reflections (c).

This behaviour could be interpreted by adding a term due to the diffuse scattering

$$R^S = K(T/\cos\theta_B)|F_g|^2 \qquad (3.1)$$

to (2.9), where K is a scaling constant relative to R. With the use of a small aperture S, the contribution of R^S could be reduced to some extent relative to the examples of Figs. 2(b) and (c). In practice, however, the extremum angular position φ_n (which will be explained in the next section) is not altered in such cases. For this reason, and to make sure of avoiding an undesirable discrimination in favour of the Bragg-reflected beam, the aperture of 3 mm diameter was used throughout the experiment as mentioned in § 3.2.

The abscissa scale $(\cos\varphi)^{-1}$ is easily converted to the t scale by $t = T/\cos\varphi$, where T is the normal thickness of the crystal. Henceforth, the curve illustrated in Fig. 2 and the one converted to the t scale will be denoted by $R(\varphi)$ and $R(t)$, respectively. They are the basis on which the structure factor is determined.

4. Procedures for determining $|F_g|$

4.1. *The determination of the fringe position*

Here, the fringe positions denoted by φ_n and t_n mean the values of φ and t at the extrema of $R(\varphi)$ and $R(t)$, respectively. The index n denotes the order of the extremum.

To determine t_n, a method of least squares was applied to a set of several (R_i, t_i) values near t_n in the $R(t)$ curve. In this case, the local profile of $R(t)$ was approximated by the quadratic form

$$R_i = \alpha_n + \beta_n(t_i - t_n)^2 \qquad (4.1)$$

for practical convenience.

4.2. *The precise determination of* λ

Before describing the determination of Λ, we shall describe how to obtain the wavelength λ used in the Bragg reflection. It can be approximately given by the peak channel number of the MCA. The integral channel number, however, is too coarse for our purpose. The non-integral (true) peak position on the channel scale was determined by a method of least squares from a set of intensity data recorded in several channels near the peak. Here, a Gaussian form was assumed for the intensity distribution. Because the wavelength was slightly changed from the standard λ_0 during the φ scanning, we had to determine λ_n for each extremum of $R(\varphi)$.

Next, one needs a formula to transform the channel scale (N) to the wavelength (λ). The following linear relation was assumed:

$$N = a(1/\lambda) + b. \qquad (4.2)$$

From the use of 220 and 440 reflections, remembering that the relevant wavelength of the former (~0·8 Å) must be precisely double that of the latter (~0·4 Å), one can determine the parameter b. Under the same SSD conditions, the spectrum of an ^{241}Am radioactive source ($\lambda = 0{\cdot}4706$ Å)* was recorded simultaneously in the MCA. From the value of N, one can determine the parameter a. No temperature effect was recognized between 288 and 298 K on these parameters. Unfortunately, however, a slight aging effect in a and b and a slight intensity dependence in b were recognized. Occasionally, therefore, the parameters were revised and the intensity dependence was empirically corrected when the total counting number was too large. As a whole, the error in λ was estimated to be 0·03% in the range near 0·4 Å.

4.3. *The determination of* Λ

Finally, we shall describe the method of least squares of determining Λ [(2.4) and (2.7)] with the use of a set of experimental data (λ_n, t_n). For this purpose the quantity

$$\xi_n = 2\pi\kappa_n t_n/\Lambda = 2\pi\kappa_n T/\Lambda\cos\varphi_n \qquad (4.3)$$

is defined, where λ_0 is used in Λ and

$$\kappa_n = \lambda_0/\lambda_n. \qquad (4.4)$$

A systematic but constant error is anticipated in φ_n because the vertical position of the specimen is not precisely known. For this reason, henceforth, φ_n in (4.3) will be replaced by $\varphi_n - \Delta\varphi$, in which $\Delta\varphi$ is dealt with as a small unknown parameter.

The problem is what theoretical quantity, let us say $\bar{\xi}_n$, must be identified with the experimental ξ_n in the method of least squares. Naively, it would be the extremum position of the theoretical curve $R(\xi)$ given by (2.9). Bearing in mind the procedure for determining t_n, however, it is more reasonable to take the extremum value $\bar{\xi}_n$ of a quadratic form representing $R(\xi)$ near the extremum, just as in the case of t_n. Care has been taken to ensure that the ranges of ξ and t multiplied by $2\pi\kappa_n/\Lambda$ are nearly the same with the use of an approximate Λ value.

The justification for this is not very straightforward because the experimental $R(t)$ is actually different from the theoretical $R(\xi)$ at least by the additional term R^S (3.1). Moreover, the exact correspondence between the ξ and t scales is unknown. We simulated $\bar{\xi}_n$ by assuming reasonable contributions of R^S and a different set of $(R_i, \xi_i + \delta)$ where δ is a small but arbitrary constant. Through this computer simulation, it was confirmed that $\bar{\xi}_n$ is not altered more than 0·01%.

Once the numerical value $\bar{\xi}_n$ is obtained, the residual, having the form

$$\xi_n - \bar{\xi}_n = (2\pi\kappa_n T/\cos\varphi_n)[1 + (\tan\varphi_n)\Delta\varphi](1/\Lambda) - \bar{\xi}_n, \qquad (4.5)$$

* $V = 26{\cdot}345 \pm 0{\cdot}001$ keV (Nelson & Saunders, 1970).

Table 2. *Present results for the structure factor*

hkl	f_{ob} (293 K)	*hkl*	f_{ob} (293 K)
111	10·6298 (5) [1]	642	3·6776 (14) [1]
220	8·4179 (6) [9]	553*	3·5312 (14) [1]
311	7·7134 (10) [1]	731	3·5176 (11) [1]
400	7·0293 (4) [1]	800	3·2784 (10) [1]
331	6·7571 (9) [1]	733*	3·1519 (14) [1]
422	6·1382 (5) [1]	660	2·9354 (6) [3]
333	5·8041 (6) [1]	822	2·9355 (15) [2]
511	5·8232 (6) [1]	555	2·8246 (27) [3]
440	5·3606 (7) [7]	751	2·8248 (25) [1]
531	5·0937 (17) [1]	840	2·6437 (7) [2]
620	4·6984 (9) [1]	753	2·5508 (29) [1]
533*	4·4825 (11) [1]	911*	2·5559 (8) [1]
444	4·1470 (12) [3]	664	2·3907 (9) [2]
551	3·9637 (14) [1]	844	2·1798 (15) [1]
711*	3·9547 (22) [1]	880	1·5514 (18) [2]

$f_{ob} = F_{ob}/Q$ [$Q = 8$ (even order): $4\sqrt{2}$ (odd order)]. ( ): probable error. [ ]: the number of the experiment.
* Corrected by the factor $(1+10^{-3})^{-1}$ from the original value.

can be assumed to be statistically random so that the method of least squares is straightforwardly applied to the above expression. Here, two parameters, $(1/\Lambda)$ and $(\Delta\varphi/\Lambda)$, are dealt with as unknown parameters and others are known experimentally with sufficient accuracy. Finally, the structure factor $|F_g|$ is determined from $(1/\Lambda)$ through the real part of (2.4) with λ_0 instead of λ.

5. Miscellaneous corrections

In the present accurate determination, one needs a few corrections to obtain the final result of $|F_g|$. The values listed in Table 2 are the corrected ones.

5.1. *Temperature*

Each $\pm\varphi$ scanning was carried out within ±1 K. The experiment at large, however, was performed in a range between 294·2 and 298·0 K. The original value, therefore, was converted to the value at 293 K assuming the M value given by (2·6*d*). The conversion factor exceeded 0·05% in some higher-order reflections.

5.2. *The polarization of the incident beam*

Since continuous X-rays were used in the present work, the natural polarization may not be assumed *a priori*. In fact, Olsen, Buras, Jensen, Alstrup, Gerward & Selsmark (1978) have measured the degree of polarization D for Cu and W targets in the range of $V/V_c = \lambda_c/\lambda$ from 0·5 up to 0·8 (V represents the electron volts corresponding to λ, V_c is the applied voltage and λ_c is the corresponding wavelength). According to them, D is estimated to be around 0·1 for Cu, and less than that for W.

To discover the importance of polarization in our own case, $R(\varphi)$ curves were measured for $V_c = 40$ and 55 kV with fixed $\lambda = 0{\cdot}4$ Å ($V = 31$ kV) as a case study. It was determined that (i) the difference between the different V_c's is detectable near the fading region (FR)* and (ii) the deviations are opposite on both sides of the FR. Similar results were also found for a Cu target. Thus, it is clear that the polarization must be properly taken into account.

The difficulty is that the D value is not precisely known. It depends on the operating conditions of the X-ray generator employed: for example the magnitude of voltage ripples and the surface contamination of the target. In practice, however, the final result of Λ with the use of different D values was not significantly altered except for a few special cases (some of 220 and 333) under the standard conditions ($\lambda = 0{\cdot}4$ Å, $V_c = 50$ kV). This is to be expected because Λ is a kind of averaged value for many fringe positions and the minute deviations in t_n are cancelled out favourably owing to (ii).

It must be emphasized, however, that the standard deviation of Λ in the least squares (§ 4.3) was significantly reduced with the value of $D \simeq 0{\cdot}1$ in many cases. In some cases, the reduction amounts to nearly half of the standard deviation on the assumption of $D = 0$. The figures listed in Table 2 are determined from a $\bar{\xi}_n$ calculated with $D = 0{\cdot}1$.

5.3. *The strain in the specimen*

The most harmful cause of errors in the *Pendellösung* method is the long-range strain gradient in the specimen, as fully discussed by Kato (1969) and Aldred & Hart (1973*a*). Such a strain gradient is usually brought about by improper surface treatment and in mounting the specimen. It causes an apparent increase of the structure factor, particularly for higher-order reflections. The short-range fluctuation of the lattice over distances much less than the extinction distance may not be harmful, although the experimental evidence is still obscure. Theoretically, it will cause a decrease in the effective Debye–Waller factor (Kato, 1980).

In the present work, after mounting the specimen, the homogeneity of the intensity profile was checked for different positions of the specimen. Also, in each experiment, the symmetric behaviour of $R(\pm\varphi)$ profiles was examined for higher-order reflections. If any anomalous asymmetry was detected, the specimen itself or the mounting was renewed.

None of these tests, however, may guarantee absolutely the strain-free condition. After all the data were collected, we examined the relative deviations $\delta = (|F_g| - \langle|F_g|\rangle)/\langle|F_g|\rangle$ for each specimen, where $\langle|F_g|\rangle$ is the mean value of $|F_g|$ determined by the use of different specimens. No systematic trend was detected except for specimen V. In this case, the

* A beating effect of the σ and π modes of the diffracted beam (Hattori, Kuriyama & Kato, 1965; Hart & Lang, 1965).

relative deviations were positive and increased slightly on increasing the order of reflections, as shown in Fig. 3. Presumably, this situation is caused by the long-range strain mentioned above.

Unfortunately, the net planes marked * in Table 2 were measured only with the use of specimen V. For this reason, in Table 2, the observed structure factors of these planes are reduced by a factor $(1+\delta_0)^{-1}$ with $\delta_0 = 10^{-3}$ (see Fig. 3).

6. Discussion

6.1. *Dawson's formalism for the generalized structure factor*

It seems appropriate to review here Dawson's theoretical framework (Dawson, 1967*a*, *b*, *c*), which enables us to deal quite generally with the anisotropy in the bonding charge and the thermal vibration of the crystal although it is based on a rigid-atom model. For concreteness, our concern is confined within the case of the diamond structure in which every atom locates at the $\bar{4}3m(T_d)$ symmetry site. Although the atomic species is identical, the atoms fall into two groups, *A* and *B*, depending on the neighbors. We shall adopt the origin of coordinates mid-way between the bonding atoms, *i.e.* at the inversion point. First, the anomalous-dispersion term is neglected for simplicity.

According to Dawson's theory, the structure factor is given by

$$F(\mathbf{g}) = 8[(f_c T_c - f_a T_a)\cos 2\pi\varphi + (f_c T_a + f_a T_c)\sin 2\pi\varphi] \qquad (6.1)^*$$

where **g** is the reflection vector specified by *h*, *k* and *l*, and

$$\varphi = \tfrac{1}{8}(h+k+l). \qquad (6.2)$$

The other symbols have the following meaning: The suffices *c* and *a* indicate the symmetric and antisymmetric components respectively of the static charge distribution $\rho(\mathbf{r})$ associated with an atom and the statistical distribution of the nucleus $t(\mathbf{r})$ due to thermal vibration. Then the Fourier transforms of $\rho(\mathbf{r})$ and $t(\mathbf{r})$ can be written in the forms

$$f(\mathbf{g}) = f_c(\mathbf{g}) + i f_a(\mathbf{g}), \qquad (6.3a)$$

$$T(\mathbf{g}) = T_c(\mathbf{g}) + i T_a(\mathbf{g}). \qquad (6.3b)$$

f_c and f_a *etc.* in (6.1) are these functions of **g**.

The *c* component, ρ_c, and consequently the Fourier transform f_c, are divided further into two components as

$$\rho_c = \bar{\rho}_s + \delta\rho_c, \qquad f_c = \bar{f}_s + \delta f_c \qquad (6.4a,b)$$

where $\bar{\rho}_s$ denotes the spherically symmetric component and $\delta\rho_c$ is the remainder which represents the angular dependence of ρ_c. Obviously, $\bar{\rho}_s$ and $\bar{f}_s$ are the dominant parts of $\rho(\mathbf{r})$ and $f(\mathbf{g})$, respectively. The model neglecting $\delta\rho_c$ and ρ_a is the standard spherical model (SSM) which is popular in ordinary structure analysis.

A similar argument can be applied to the distribution $t(\mathbf{r})$ and the Fourier transform $T(\mathbf{g})$. Dawson & Willis (1967), however, developed the theory in a more practical but less rigorous manner (see also Willis & Pryor, 1975). They obtained the formulae

$$T_c = \exp[-\beta(h^2+k^2+l^2)] \quad \text{(Debye-Waller factor)} \qquad (6.5a)$$

$$T_a = LT^2(hkl)\,T_c \qquad (6.5b)^*$$

where *L* is a positive constant independent of *h*, *k* and *l*, and *T* is the absolute temperature. It is worth pointing out that the (*h*, *k*, *l*) dependence of f_a is similar to (6.5*b*), according to Dawson. In the following, reflection planes are classified into (I), (II) and (III) according as $h+k+l = 4n$, $4n+2$ and $4n\pm1$. The phase factors $\cos 2\pi\varphi$ and $\sin 2\pi\varphi$ are listed in Table 3 for these three cases.

This review will be closed by pointing out the semi-quantitative properties of $\bar{f}_s$, f_a *etc.* First of all, it is anticipated that $\bar{f}_s \gg f_a > \delta f_c$ and $T_c \gg T_a$. For this reason, the term $f_a T_a$ can be neglected in (6.1). Additionally, the anisotropic terms f_a and δf_c decrease more rapidly with $|\mathbf{g}|$ than the spherical term $\bar{f}_s$ because the former arise mainly from the rearrangement of electrons in the outer shell.

Based on the above arguments one can summarize the characteristic aspects of the structure factor as follows.

(i*a*) In type (I), the antisymmetric component $(f_c T_a + f_a T_c)$ does not contribute to $F(\mathbf{g})$, absolutely (see Table 3).

* Dawson's structure factor is distinguished from F_g by using $F(\mathbf{g})$.

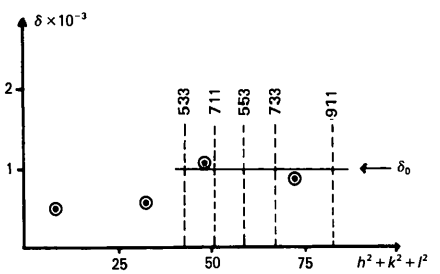

Fig. 3. The determination of the correction factor. $\delta = (|F| - \langle|F|\rangle)/\langle|F|\rangle$ is plotted for *hkl* reflections in which many $|F|$ values are available by using different specimens. δ_0 is the mean value of δ in the range of $(h^2+k^2+l^2)$ concerned and it was estimated to be 10^{-3}. The correction factor for the five planes indicated was given by $(1+\delta_0)^{-1}$.

* In the theory of Dawson & Willis, it would be better to call T_a an 'anharmonic temperature factor'.

Table 3. *The phase factor in equation* (6.1)

Type	$h+k+l$	$\cos 2\pi\varphi$	$\sin 2\pi\varphi$
I	$4n$	$(-1)^n$	0
II	$4n+2$	0	$(-1)^n$
III	$4n\pm1$	$(-1)^n/(2)^{1/2}$	$\pm(-1)^n/(2)^{1/2}$

(i*b*) Nevertheless, the centrosymmetric but non-spherical component (δf_c) may have effects in the lower-order (L) reflections.

(ii) Type (II), which is forbidden in SSM, is observable through the term ($f_cT_a+f_aT_c$).

(iii*a*) In type (III), both ($f_cT_a+f_aT_c$) and δf_c contribute to $F(\mathbf{g})$.

(iii*b*) In this case, however, only ($f_cT_a+f_aT_c$) has effects for the middle-order (M) reflections, particularly if the product (hkl) is large [see (6.5*b*) and the comment].

(iv) For the higher-order (H) reflections the anisotropic terms cease contributing in any type of reflections so that the structure factor must be normal.

Finally, if one takes into account the anomalous dispersion and the nucleus Thomson scattering (f_{NT}), one has to replace f_c by $f_c+f'+f_{NT}+if''$. No modification is required to the antisymmetric component. Then the observable structure factor must be

$$|F_g| = Q[(f_c+f'+f_{NT})T_c + (f_aT_c+f_cT_a)\tan 2\pi\varphi]. \quad (6.6)$$

6.2. *The interpretation of the present data set*

To elucidate the physical implications of the data set, remembering (6.6) we shall be concerned with the deviation from the SSM defined by

$$\Delta = f_{obs} - f_{th}T_c, \quad (6.7a)$$

$$f_{th} = f_{HF}+f'+f_{NT}. \quad (6.7b)$$

Here, f_{HF} is the scattering factor of the isolated atom and was recalculated by S. Wako directly from the non-relativistic Hartree-Fock wave function (Clementi, 1965), without using any interpolation method. This was necessary to analyze the data set with the present accuracy. The values are listed in Table 4.

For the real part of the anomalous-dispersion term f', we adopted Cromer & Liberman's (1970, 1981) values. Although the correctness of these was tested experimentally by Takeda & Kato (1978), recently Jensen (1979) proposed the necessity for a λ-dependent term. For this reason, we examined carefully the λ dependence of $|F_g|$ for some reflections. As a result, we arrived at the same conclusion as Takeda & Kato. Also, theoretically, Jensen's term is cancelled out by another term of the same order of magnitude. These results will be reported elsewhere (Saka, Omote & Kato, 1986).

The β value in T_c (6.7*a*) was fixed at 3.877×10^{-3} by the method of least squares in the Wilson plot of our own data for the reflections of type (I) higher than 642. Incidentally, if one uses ten data over 620, the β value becomes 3.869×10^{-3}.

In the second column of Table 5, Δ/f_{HF} is listed. As anticipated, there are appreciable deviations in the L reflections (up to 444) of both type (I) and (III), which definitely exceed the error limit (0·1%).

In the range of M and H reflections (over 551), the deviation for type (I) is less than 0·1% except for the 664 reflection, which might include minute experimental errors. If one admits the conclusions (i*a*) and

Table 4. *The non-relativistic HF structure factor*

hkl	f_{HF}	hkl	F_{HF}
111	10·5286	642	4·5480
220	8·7102	553	4·4045
311	8·1644	731	4·4045
400	7·5077	800	4·1822
331	7·1833	733	4·0581
422	6·7022	660	3·8658
333	6·4392	822	3·8658
511	6·4392	555	3·7583
440	6·0350	751	3·7583
531	5·8106	840	3·5913
620	5·4637	753	3·4979
533	4·9718	911	3·4979
444	4·8054	664	3·3524
551	4·5430	844	3·1438
711	4·5430	880	2·5333

Table 5. *The comparison of Δ/f_{HF} values with those of Aldred & Hart* (1973*a*, *b*) (*AH*) *and Teworte & Bonse* (1984) (*TB*) (*unit*: 10^{-3})

hkl	Present	TB(Ag)	AH(Ag)	TB(Mo)	AH(Mo)	Mean value
111	19·6	19·5	20·5	20·6	21·3*	20·2
220	−4·9	−5·6	−5·7	−3·5	−4·0	−4·8
311	−15·5	−15·9	−14·9	−15·4	−15·1	−15·3
400	−5·7	−6·2	−6·0	−7·1	−6·5	−6·2
331	9·5	9·9	9·8	8·2	9·9	9·7
422	2·4	1·4*	2·1	3·6	5·1*	2·7
333	−1·6	−0·9	−1·3	−0·7	0·2*	−1·0
511	1·3	0·5	0·8	1·6	1·4	1·2
440	2·4	2·9	3·1	2·5	2·7	2·7
531	1·0					
620	0·9					
533	1·3					
444	1·1	0·9*	2·5	2·9*	2·3	1·9
551	1·4	0·4	0·9	0·5	2·6*	0·9
711	−0·5					
642	0·8					
553	3·1					
731	0·0					
800	0·5	−2·7†		−0·1		(0·1)
733	2·2					
660	−0·4	0·3	1·9†	1·6†	1·6†	(−0·0)
822	−0·4					
555	0·5	1·0	−0·4	0·8	−0·5	0·3
751	0·5					
840	−0·7					
753	0·9					
911	2·3					
664	−1·4					
844	0·4	−0·2	−1·4†	2·5†	−2·6†	(0·1)
880	−0·5	1·9†	3·0†		0·2	(−0·1)

$\Delta = f_{ob}-f_{th}T_c$, $f_{th}=f_{HF}+f'+f_{NT}$, f_{HF}: Wako's value. $f'=0·013$ (0·4 Å), 0·016 (0·415 Å), 0·042 (Ag $K\alpha$), 0·072 (Mo $K\alpha$). $f_{NT}=0·004$.

Mean value: The average of the values without the use of the two extremum values. * indicates values which deviate more than 0·1% from the mean value. † indicates values omitted to obtain the mean value in ( ) for the reason explained in the text (§ 6.4).

(iv) in § 6.1, this result is very satisfactory. We notice, however, a systematic trend that, in some reflections of type (III), the deviation is larger than 0·1%. We shall return to this point in §§ 6.3 and 6.5.

6.3. *The anharmonicity of the thermal vibration*

At this stage, it is worth discussing to what extent the anharmonic term T_a contributes to the structure factor $F(\mathbf{g})$. For this purpose, we shall refer to the neutron work on the 222 forbidden reflection (Keating, Nunes, Batterman & Hastings, 1971; Roberto, Batterman & Keating, 1974). In this case, (6.1) and (6.5) reduce to

$$F(222) = -8bT_a, \qquad T_a = 8T^2LT_c \qquad (6.8a,b)$$

respectively, where b is the nucleus scattering amplitude ($f_c = b$; $f_a = 0$) of neutrons. The above authors confirmed a T^2 dependence by measuring the integrated intensity in the range above the Debye temperature (~540 K). One then obtains $L = 1{\cdot}7 \times 10^{-10}$ (°)$^{-2}$. With this value, one can evaluate T_a for other reflections at room temperature by assuming the extrapolation of the T^2 dependence. Then the following results are obtained:

$$T_a = 1{\cdot}4 \times 10^{-3} \qquad 555$$
$$= 1{\cdot}1 \times 10^{-3} \qquad 753$$

and others are less than 0·1%.

From (6.1) and Table 3, the structure factor for the M and H reflections can now be written in the form

$$f(\mathrm{III}, M+H) = f_cT_c \pm (f_cT_a + f_aT_c), \quad (6.9a)$$

where the double signs must be selected in accordance with those of $h+k+l = 4n \pm 1$. On the other hand, we already know that $f(\mathrm{I}, M+H) = f_cT_c$ is well described by $f_{\mathrm{HF}}T_c$. Therefore, it is safe to assume that

$$\Delta/f_{\mathrm{HF}} = \pm[T_a + (f_a/f_{\mathrm{HF}})T_c] \qquad (6.9b)$$

for M and H reflections. Compared with the experimental values in Table 5, the anisotropic term T_a is buried in the charge anisotropy [the second term of (6.9)]. In fact, Δ/f_{HF} must be negative for 555 and 753 if the deviation is caused purely by the thermal anisotropy.

Finally, it is emphasized that the effect of the charge rearrangement is not confined to L reflections in the present level of accuracy. This implies that the charge distribution near the nucleus is also slightly modified by making the bond.

6.4. *Comparison with previous work*

Extensive work comparable to ours has been reported by Aldred & Hart (1973*a*) and very recently by Teworte & Bonse (1984). Others are less accurate or only a few reflections are measured so that they are not discussed here. Also, the result of Aldred & Hart at low temperature is not compared because the present value of β cannot be applied to it.

The Δ/f_{HF} values calculated on the same basis as ours are listed in Table 5. The mean value without the use of the maximum and minimum among the five data sets is listed in the last column. The present data set falls in the range of ±0·1% from the mean value. Incidentally, the mark * denotes values outside this range. As discussed before, higher-order reflections like 660 must be normal. For the same reason, the largely scattered values for 844 and 880 in the data sets of Aldred & Hart and Teworte & Bonse are probably due to some errors. It seems, therefore, reasonable to put the values marked with a † out of consideration. We believe that our data set is slightly better than theirs.

Nevertheless, if one examines the values without a * the agreement among the five data sets is remarkable. The accuracy level of the mean value is probably of order 0·05% or even better in some low-order reflections up to 440. In the higher-order reflections, it is safe to say that the present result stays on the level of 0·1%. It is worth mentioning that each of the methods employed by the three groups belongs to a different category as mentioned in the *Introduction.* This indicates that the method of *Pendellösung* oscillation is very reliable for the accurate determination of structure factors.

6.5. *The difference Fourier analysis*

So far, the observed data set was analyzed directly through the (h, k, l) dependence. In this section, the quality of our data will be discussed in terms of difference Fourier analysis. Since our data set covers higher-order reflections it is anticipated that a reasonably true picture will be obtained of the redistribution of the charge in the crystal. For this purpose, the forbidden reflection must be amended from other sources. We borrowed the values: $|F|$ (at 293 K) = 1·645(34) (Fehlman & Fujimoto, 1975) for the 222 and 0·035(2) for the 442 reflection (Trucano & Batterman, 1972).

Fig. 4 illustrates the difference of the charge density from SSM under the harmonic oscillation. The bonding charge is clearly seen (max. = 0·221 e Å^{-3}) in the vicinity of the middle point M between the nearest atoms and the deficit in the anti-bonding region (min. = −0·080 e Å^{-3}) (see Fig. 4*a*). Moreover, the deficit is rather gradually damped towards the center C of the unit cell which is remotest from all atoms in the crystal. The deficit is recognized also along ⟨110⟩ and ⟨100⟩ directions.

Along a ⟨111⟩ direction a ripple modulation is noticeable, although it is faint. Since this situation is physically unrealistic, the behaviour would be a termination effect of the Fourier synthesis. Moreover,

a small hump is noticed (0·044 e Å^{-3}) at the atomic position A (or B). We believe that the hump is genuine, because it is larger than the amplitude of the ripple (~0·015 e Å^{-3}). Thus, more directly, one can see that the charge distribution near the atomic position is slightly enhanced in the crystal.

Concluding remarks

The structure factors of 30 reflections were experimentally obtained with an accuracy level of 0·1%. Our data set agrees reasonably well with the Aldred & Hart and Teworte & Bonse data sets, but seems slightly better. Through the comparison (§ 6.4), our data set of L reflections (up to 440) would probably be better than 0·05% in accuracy level, which is more than our expectation.

Methodologically, the high-intensity X-ray generator was very useful for speeding up the individual experiments and collecting many data. The method of determining the extremum positions in the $R(t)$ curve (§ 4.3) and the method of least squares (§ 4.3) using $\bar{\xi}_n$ values are significant in attaining the accuracy of this level. The method of least squares assuming equidistant positions of the oscillation is not reliable because of the fading effect of the X-ray polarization and the unknown background. At least for estimating the probable error, and for determining a precise $|F_g|$ value in some cases, the degree of polarization of the incident beam must be properly taken into account.

An extensive comparison with specific theories will be postponed until the future. Nevertheless, Dawson's theory of the generalized structure factor was very useful for examining the quality of the data set. The authors believe that the present data set and the result of the difference Fourier map may serve as the critical test of any theoretical approach to the electronic structure of silicon. This is one of the achievements of the dynamical theory which has been developed since the distinguished work of Professor P. P. Ewald.

The authors express their thanks to Professor S. Wako for his courtesy in recalculating structure factors and to Mr S. Samata for his contribution in the early stages and to Mr K. Yasuda for his efforts in operating the X-ray generator. Gratitude is also given to the Mitsubishi Foundation for financial support.

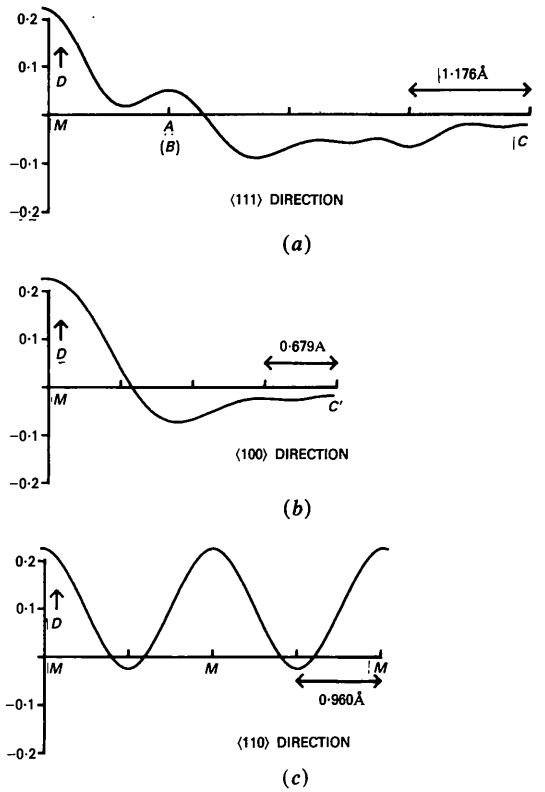

Fig. 4. The difference Fourier synthesis based on the present results in Table 5. D is the charge density (e Å^{-3}). (*a*) Along ⟨111⟩; (*b*) along ⟨100⟩; (*c*) along ⟨110⟩. $A(B)$ denote the atomic positions, M is mid-way between atoms A and B. C represents the center of the unit cell, $(\frac{1}{2}, \frac{1}{2}, \frac{1}{2})$. $C' = (\frac{1}{2}, 0, 0)$, which is equivalent to C.

References

ALDRED, P. J. E. & HART, M. (1973*a*). *Proc. R. Soc. London Ser. A*, **332**, 223–238.

ALDRED, P. J. E. & HART, M. (1973*b*). *Proc. R. Soc. London Ser. A*, **332**, 239–254.

AZAROFF, L. V. (1974). *X-ray Diffraction*, Appendix *4A*. New York: McGraw Hill.

CLEMENTI, E. (1965). A supplement to the paper in *IBM J. Res. Dev.* **9**, 2–19.

CROMER, D. T. & LIBERMAN, D. (1970). *J. Chem. Phys.* **53**, 1891–1898.

CROMER, D. T. & LIBERMAN, D. (1981). *Acta Cryst.* A**37**, 267–268.

DAWSON, B. (1967*a*). *Proc. R. Soc. London Ser. A*, **298**, 255–263.

DAWSON, B. (1967*b*). *Proc. R. Soc. London Ser. A*, **298**, 264–288.

DAWSON, B. (1967*c*). *Proc. R. Soc. London Ser A*, **298**, 379–394.

DAWSON, B. & WILLIS, B. T. M. (1967). *Proc. R. Soc. London Ser. A*, **298**, 307–315.

FEHLMAN, M. & FUJIMOTO, I. (1975). *J. Phys. Soc. Jpn*, **38**, 208–215.

HART, M. (1981). *J. Cryst. Growth*, **55**, 409–427.

HART, M. & LANG, A. R. (1965). *Acta Cryst.* **19**, 73–77.

HATTORI, H., KURIYAMA, H., KATAGAWA, T. & KATO, N. (1965). *J. Phys. Soc. Jpn*, **20**, 988–996.

HATTORI, H., KURIYAMA, H. & KATO, N. (1965). *J. Phys. Soc. Jpn*, **20**, 1047–1050.

JENSEN, M. S. (1979). *Phys. Lett.* **74A**, 41–44.

KATO, N. (1968). *J. Appl. Phys.* **39**, 2231–2237.

KATO, N. (1969). *Acta Cryst.* A**25**, 119–128.

KATO, N. (1980). *Acta Cryst.* A**36**, 763–769.

KEATING, D. T., NUNES, A., BATTERMAN, B. W. & HASTINGS, J. (1971). *Phys. Rev. B*, **4**, 2472–2478.

NELSON, G. C. & SAUNDERS, B. G. (1970). *Nucl. Instrum. Methods*, **84**, 90–92.

OLSEN, J. S., BURAS, B., JENSEN, T., ALSTRUP, O., GERWARD, L. & SELSMARK, B. (1978). *Acta Cryst.* A**34**, 84–87.

ROBERTO, J. B., BATTERMAN, B. W. & KEATING, D. T. (1974). *Phys. Rev. B*, **9**, 2590–2599.

SAKA, T., OMOTE, K. & KATO, N. (1986). In preparation.

TAKAMA, T., IWASAKI, M. & SATO, S. (1980). *Acta Cryst.* A**36**, 1025-1030.
TAKEDA, T. & KATO, N. (1978). *Acta Cryst.* A**34**, 43-47.
TANEMURA, S. & KATO, N. (1972). *Acta Cryst.* A**28**, 69-80.
TEWORTE, R. & BONSE, U. (1984). *Phys. Rev. B*, **4**, 2102-2108.
TRUCANO, P. & BATTERMAN, B. W. (1972). *Phys. Rev. B*, **6**, 3659-3666.
UTEMISOV, K., SHIL'SHTEIN, S. SH. & SOMENKOV, V. A. (1981). *Kristallografiya*, **26**, 182-185. [*Sov. Phys. Crystallogr.* **26**(1), 101-102.]
UTEMISOV, K., SOMENKOVA, V. P., SOMENKOV, V. A. & SHIL'SHTEIN, S. SH. (1980). *Kristallografiya*, **25**, 845-849. [*Sov. Phys. Crystallogr.* **25**(4), 484-487.]
WILLIS, B. T. M. & PRYOR, A. W. (1975). *Thermal Vibrations in Crystallography*. Cambridge Univ. Press.

Acta Cryst. (1986). A**42**, 478-481

X-ray Birefringence and Forbidden Reflections in Sodium Bromate

BY DAVID H. TEMPLETON AND LIESELOTTE K. TEMPLETON

Department of Chemistry, University of California, Berkeley, CA 94720, *USA*

(*Received* 13 *February* 1986; *accepted* 17 *April* 1986)

Abstract

Reflections forbidden by a screw-axis rule are observed in sodium bromate with synchrotron radiation near the bromine K absorption edge, where X-ray birefringence occurs. The intensities vary with azimuthal angle according to theoretical predictions and indicate a larger magnitude for the birefringence than did earlier experiments. This technique is a method of selective diffraction in which atoms of a single element in a single chemical state contribute to the signal, and it can reveal their positions with precision.

1. Introduction

One effect of X-ray dichroism and birefringence is that the screw-axis and glide-plane rules for absent reflections are not rigorous (Templeton & Templeton, 1980; Dmitrienko, 1983, 1984). Atoms which are related by one of these symmetry elements may have different scattering factors if the orientations of their susceptibility tensors are different with respect to the polarization vectors of the photons. The rules depend on exact cancellation of scattering from these atoms.

We first observed reflections forbidden by a screw-axis rule in diffraction experiments with sodium bromate near the bromine K absorption edge (Templeton & Templeton, 1985, hereafter TT85), but lacked time then to study them in detail. Here we report some further experiments which confirm the novel dependence of these reflections on azimuthal angle and thus support the validity of the optical model which we have been using. This phenomenon offers a new method of selective diffraction in which atoms of only a single element contribute to the signal. The experiments show that the signals are strong enough to be observed without exceptional difficulty, and demonstrate that they can give accurate information about structure.

Because the method requires X-rays with a wavelength close to an absorption edge, and intense beams of such radiation are most readily available at a synchrotron source, we did this work at the Stanford Synchrotron Radiation Laboratory (SSRL). Although the effect arises from polarization-dependent properties, it turns out that polarized radiation is not needed. Nor are the requirements for narrow spread of wavelength and for high intensity particularly severe. Thus, similar experiments may be possible with more conventional sources.

2. Theory

In sodium bromate the bromine atoms are on threefold axes in the special positions of $P2_13$, with $x = 0{\cdot}40640\,(3)$ (TT85):

$$x, x, x; \tfrac{1}{2}+x, \tfrac{1}{2}-x, -x;$$
$$-x, \tfrac{1}{2}+x, \tfrac{1}{2}-x; \tfrac{1}{2}-x, -x, \tfrac{1}{2}+x.$$

We describe the scattering factor of each atom by a tensor with principal values f_π, f_π, and f_σ (complex numbers), oriented with f_σ parallel to the respective threefold axis. In the coordinate system of the cubic unit cell, these tensors are:

$$\mathbf{f}_1=\begin{pmatrix} a & b & b \\ b & a & b \\ b & b & a \end{pmatrix}, \quad \mathbf{f}_2=\begin{pmatrix} a & -b & -b \\ -b & a & b \\ -b & b & a \end{pmatrix},$$
$$\mathbf{f}_3=\begin{pmatrix} a & -b & b \\ -b & a & -b \\ b & -b & a \end{pmatrix}, \quad \mathbf{f}_4=\begin{pmatrix} a & b & -b \\ b & a & -b \\ -b & -b & a \end{pmatrix}, \tag{1}$$

$$a = f_0 + f' + if'' = (f_\sigma + 2f_\pi)/3, \tag{2}$$

$$b = (f_2' + if_2'')/3 = (f_\sigma - f_\pi)/3, \tag{3}$$

0108-7673/86/060478-04$01.50